Research Article

Study of *Lycium barbarum* in the Treatment of Osteoradionecrosis of the Jaw: An Integration of Network Pharmacology With Experimental Validation

Liyuan Fan[1,2,3], Jinghan Wang[2,3], Zhongchao Wang[3,4], Liang Shi[2,3], Linya Zeng[1], Yandong Mu[1,*]

[1]Department of Stomatology, Sichuan Provincial People's Hospital, School of Medicine, University of Electronic Science and Technology of China, 611731 Chengdu, Sichuan, China
[2]Department of Prosthodontics, The Affiliated Stomatology Hospital, Southwest Medical University, 646000 Luzhou, Sichuan, China
[3]Oral & Maxillofacial Reconstruction and Regeneration of Luzhou Key Laboratory, 646000 Luzhou, Sichuan, China
[4]Department of Periodontics & Oral Mucosal Diseases, The Affiliated Stomatology Hospital, Southwest Medical University, 646000 Luzhou, Sichuan, China
*Correspondence: yandongmu@126.com (Yandong Mu)
Academic Editor: Mehmet Ozaslan
Submitted: 14 July 2025   Revised: 22 September 2025   Accepted: 29 September 2025   Published: 30 October 2025

Abstract

Background: Osteoradionecrosis of the jaw (ORNJ) is a common complication following radiotherapy for head and neck cancer. Thus, this study aimed to explore the effects of active components in *Lycium barbarum* on ORNJ through network pharmacology and to conduct experimental verification to identify potential therapeutic targets. **Methods**: The main active ingredients in *Lycium barbarum* (Gouqi), a traditional Chinese herbal medicine, was used in this study. After identifying ferroptosis-related genes associated with ORNJ, we performed Gene Ontology (GO) and Kyoto Encyclopedia of Genes and Genomes (KEGG) enrichment analyses and constructed an interaction network. A molecular interaction force analysis was then performed on eight binding conformations to identify the optimal conformation with the lowest binding free energy. We established a model of ORNJ in *Sprague-Dawley* (SD) rats and administered oral *Lycium barbarum* glycopeptide (LbGP) to the experimental group. Moreover, reverse transcription quantitative polymerase chain reaction (RT-qPCR), enzyme-linked immunosorbent assay (ELISA), and immunohistochemical staining techniques were then employed to detect the mRNA and protein levels of various relevant cytokines. **Results**: Based on network pharmacology predictions, this study identified three potential active components in *Lycium barbarum*, namely β-sitosterol, glycitein, and quercetin. The possible effects of these components in the treatment of ORNJ were analyzed. Seven hub genes related to ferroptosis and ORNJ were identified, and LbGP was selected for *in vivo* verification. The expression levels of *TP53*, *EGFR*, *IL-6*, and *TNF* were significantly altered in the LbGP group compared to the untreated group, as revealed by the qPCR, ELISA, and immunohistochemistry assays. **Conclusion**: The use of *Lycium barbarum* extract may exert therapeutic effects on mandible injury following ORNJ by regulating the expression of *TP53*, *EGFR*, *IL-6*, and *TNF*.

Keywords: osteoradionecrosis; lycium; network pharmacology; ferroptosis

1. Introduction

Osteoradionecrosis of the jaw (ORNJ) is a critical complication related to the treatment of head and neck cancer, with an incidence ranging from 5.4% to 13% [1]. Indeed, ORNJ is considered to be one of the particularly severe complications among the potential adverse reactions of extensive high-dose radiation therapy in the oral cavity, maxilla, mandible, and salivary glands. Moreover, the primary feature of ORNJ is a non-healing, exposed bone area that can occur without affecting the mucosa or skin [2]. The etiology and pathogenesis of ORNJ remain uncertain and are associated with factors such as radiation trauma and infection, bone injury, and the three-low theory [3]. Presently, no universally accepted treatment protocol exists for ORNJ, with current treatment options ranging from conservative approaches (such as antibiotics, antifibrotic agents, and antioxidants) to radical surgical interventions and/or hyperbaric oxygen therapy (HBO). The selection of treatment is based on the severity of clinical presentations.

Lycium barbarum (Gouqi) is a traditional Chinese medicinal herb containing various chemical components, including polysaccharides, flavonoids, anthocyanins, and alkaloids. Notably, *Lycium barbarum* has multiple pharmacological effects, including immune regulation, anti-aging, blood sugar and lipid level regulation, blood pressure reduction, anti-tumor properties, and the potential to reduce inflammatory responses.

Notably, ferroptosis, a form of regulated cell death distinct from apoptosis, necrosis, and autophagy, has recently emerged as a critical mechanism in various diseases [4]. Growing evidence highlights the role of ferroptosis in mediating cellular damage and inflammatory responses, sug-

gesting its potential relevance in the progression of ORNJ. Moreover, primitive radioresistant cancer cells can become radiosensitive through the inhibition of ferroptosis using Solute Larrier Camily 7 member 11 (*SLC7A11*) or Glutathione Peroxidase 4 (*GPX4*) inhibitors [4].

Lycium barbarum polysaccharide (LBP) is a key biologically active component of *Lycium barbarum*, functioning as an antioxidant and preventing cell death due to oxidative stress [5]. *Lycium barbarum* glycopeptide (LbGP) is derived and purified from LBP and consists of five glycopeptides with strong immunomodulatory and anti-aging properties. Our previous study demonstrated that LbGP regulates oxidative stress and ferroptosis through the Nrf2 pathway and ameliorates epithelial injury induced by ionizing radiation [6]. Nonetheless, the precise molecules in *Lycium barbarum* that are associated with ferroptosis in ORNJ remain unknown. Therefore, this study aimed to investigate the interplay between disease targets, active compounds of *Lycium barbarum*, and the relevant pathways by leveraging network pharmacology. Correlations between this herbal medicine and ferroptosis-linked radiogenic mandibular osteomyelitis should enhance our understanding of the mechanism of action through which *Lycium barbarum* functions at the molecular level.

2. Materials and Methods

2.1 Composition of Lycium barbarum

The Traditional Chinese Medicine Systems Pharmacology Database and analysis platform (TCMSP) (https:tcmsp-e.com/tcmsp.php) [7] is based on the traditional Chinese Medicine Systems pharmacology framework. The TCMSP includes 837 related disorders, 29,384 constituents, 3311 targets, and 499 varieties of Chinese therapeutic plants from the Chinese Pharmacopeia. The TCMSP also contains 12 crucial Absorption, Distribution, Metabolism, Excretion (ADME)-associated attributes of drugs, including drug similarity, human oral bioavailability (OB), Caco-2 permeability, half-life, blood–brain barrier integrity, and compliance with Lipinski's rule-of-five for drug screening and assessment. Compositional information for *Lycium barbarum* was sourced from the TCMSP database.

2.2 Screening for Active Ingredients in Traditional Chinese Medicine

ADME [8] refers to the Absorption, Distribution, Metabolism, Excretion, and Toxicity of drugs. Thus, the ADME content is applied to contemporary drug design and screening in pharmacokinetics research. This research is based on the characteristics of the ADME TCMSP databases and provides relevant data with a selected oral exploitation degree OB of >30%, and a drug-likeness (DL) value of >0.18, corresponding to a chemical composition as an efficient ingredient.

2.3 Prediction and Screening of Target Proteins for Active Ingredients in Traditional Chinese Medicine

We used a two-step procedure to predict and screen the target proteins of effective Chinese medicine ingredients. First, the TCMSP database was utilized to predict protein targets for the active components of *Lycium barbarum*. Subsequently, the predicted targets in the TCMSP database were transformed into gene names using UniProtKB (http://www.uniprot.org) [9].

2.4 Ferroptosis-Related Genes and Disease Targets for Cell Death

The GeneCards database (https://www.genecards.org/) offers extensive information on genes for individuals [10]. Therefore, we identified a total of 445 ferroptosis-related genes (FRGs) in the GeneCards database using the keyword "ferroptosis" and a relevance score of >1 as the screening criterion. Meanwhile, employing "ferroptosis" as the keyword in the Molecular Signatures Database (MSigDB, https://www.gsea-msigdb.org/gsea/msigdb/) [11] resulted in obtaining an additional 64 FRGs from the reference gene set WP_FERROPTOSIS. Additionally, we downloaded "marker", "suppressor", and "driver" genes associated with ferroptosis from the FerrDb database (http://www.zhounan.org/ferrdb/current/) [12], from which 339 human protein-coding FRGs were screened; **Supplementary Table 1** lists the FRGs from the three sources combined, yielding 626 FRGs for further analysis.

The search term "osteoradionecrosis of the jaw" was used to examine the GeneCards database. A total of 35 genes linked to ORNJ targets, with a relevance score >1, were found after screening (**Supplementary Table 2**).

2.5 Lycium barbarum Treatment and ORNJ-Related Genes

The intersection of targeted proteins for screened Chinese herbal ingredients and screening genes associated with ORNJ (ORNJ-related genes, or ORNJRGs) yielded *Lycium barbarum*.

2.6 Ferroptosis Genes Related to Osteoradionecrosis of the Jaw Bone: Associations With Lycium barbarum

The screened genes relating to ORNJ and ferroptosis were intersected to identify any FRGs in *Lycium barbarum* therapy. These were designated as hub genes. Individual proteins that interact with one another form protein–protein interaction networks. The STRING database (https://cn.string-db.org) [13] can be employed to search for connections between anticipated and existing proteins. Using this database, the biological species was set to human with a confidence level of ≥0.400, and the hub genes were used to build a protein–protein interaction network that was visualized using Cytoscape 3.9.1 (Cytoscape Consortium, San Diego, CA, USA). Additionally, genes with similar functions were also predicted, and an interplay net-

work was established through the GeneMANIA website (https://genemania.org).

2.7 Enrichment Analysis of Hub Genes

Gene Ontology (GO) analysis is a general method for large-scale functional enrichment, including both molecular functions (MFs) and biological processes (BPs). The Kyoto Encyclopedia of Genes and Genomes (KEGG) (https://www.kegg.jp) is an extensive database that contains information on genomes, illnesses, biological pathways, and drugs [14]. The R package clusterProfiler [15] was employed to perform GO annotation analysis of hub genes, with entry screening standards of p.adjust < 0.05 and a false discovery rate (FDR) value (q-value) of <0.05 using the Benjamini–Hochberg method for p-value correction.

2.8 Construction of mRNA–miRNA, mRNA–RBP, mRNA–TF, and mRNA–Drug Interaction Networks

The ENCORI database (https://rnasysu.com/encori/) [16] is version 3.0 of the starBase database. Interactions in ENCORI, including RNA-binding protein (RBP)–mRNA, RNA–RNA, ncRNA–RNA, RBP–ncRNA, miRNA–mRNA, and miRNA–ncRNA, are formulated based on CLIP-seq and degradome sequencing data specific to plants. The interplay between hub genes and miRNAs was predicted using the ENCORI database. Subsequently, the mRNA–miRNA data were screened. Three or more databases supported the establishment of this predicted mRNA–miRNA interplay network.

The CHIPBase database [17] (version 3.0) (https://rna.sysu.edu.cn/chipbase/) recognizes hundreds of thousands of binding motifs and binding sites from DNA-binding protein ChIP-seq information, while predicting transcriptional regulatory relationships between millions of genes and transcription factors (TFs). Meanwhile, TFs that bind to hub genes were identified using the CHIPBase database. Subsequently, to build an mRNA–TF interplay network, we filtered mRNA–TF data supported by four or more databases.

Additionally, the Comparative Toxicogenomics Database (CTD) [18] (http://ctdbase.org/) was used to predict underlying drugs or small-molecule compounds that interact with hub genes. Subsequently, mRNA–drug data supported by four or more databases were filtered to build an mRNA–drug interplay network.

2.9 Screening and Structural Pretreatment of Active Ingredients in Traditional Chinese Medicines

The RCSB PDB database (https://www.rcsb.org) was used to extract crystal structures for the hub genes in pdb format [19]. Core small-molecule structures were obtained in mol2 format from the TCMSP database. For crystal structures downloaded from the RCSB PDB database, we used PyMOL (https://pymol.org/2/) to remove ligands, select chains, and extract them into PDB format. Protein molecule active docking sites were predicted using Discov-

ery Studio 2.5.5 (Dassault Systèmes BIOVIA, San Diego, CA, USA). For the extracted protein structures mentioned above, the AutoDockTool-1.5.7 program (The Scripps Research Institute, La Jolla, CA, USA) [20] was utilized to eliminate water molecules, supplement hydrogen atoms, compute charges, and export files in both pdb and pdbqt formats. For the core small-molecule structures in mol2 format, we used the AutoDockTool-1.5.7 program to add hydrogen atoms, calculate charges, and determine rotatable bonds for the ligands. These formats were then exported as pdbqt format files.

2.10 Molecular Docking and Interaction Force Analysis

Autodock Vina (1.2.0, The Scripps Research Institute, La Jolla, CA, USA) [21] was utilized for docking proteins and small molecules, generating nine complex conformations for each protein–molecule docking. The docking score Affinity in AutoDock Vina indicates the strength of binding: Affinity >-4 kcal/mol represents very poor or no binding, -7 kcal/mol $<$ Affinity < -4 kcal/mol is defined as moderate binding, and Affinity <-7 kcal/mol is considered strong binding. Conformations with a binding free energy of <-5 kcal/mol were filtered through energy ranking, with the lowest binding free energy chosen as the target conformation for analysis. For all target conformations, PLIP 2021 (Freie Universität Berlin, Berlin, Germany) [22] was employed to analyze the intermolecular non-covalent interplay, such as hydrophobic interactions, hydrogen bonds, and the cation–π interplay. All interplay was visualized using PyMOL (https://pymol.org/) and saved in png format.

2.11 Transcription and Expression Levels of Inflammatory Factors in Bone Marrow Mesenchymal Stem Cells of Rats With Radiation-Induced Mandibular Osteomyelitis

Sprague-Dawley (SD) rats aged 6–8 weeks were randomly divided into the normal control (NC), ORNJ, and ORNJ + LbGP groups. To establish the ORNJ animal model, rats from the ORNJ and ORNJ + LbGP groups were irradiated once daily at doses of 7 Gy per fraction for a total of five fractions [23]. The NC rats did not receive radiation treatment. The ORNJ + LbGP rats were also administered oral LbGP at a dose of 400 mg/kg/d, whereas the NC and ORNJ rats were administered the same concentration of normal saline. After 3 weeks of radiotherapy, the first molar of the mandible was extracted under isoflurane local anesthesia. The rats were euthanized with excessive anesthesia via inhalation using isoflurane (2% concentration) delivered at 0.41 mL/min with a fresh gas flow rate of 4 L/min. The mandibular tissues were extracted, and jaw bone marrow mesenchymal stem cells (JBMMSCs) were isolated and cultured for 3–5 generations for the follow-up experiments. The identity of these cells was confirmed through morphology, surface marker expression, and differentiation ability. All the cultures were subjected to routine tests, and mycoplasma contamination was found to be negative. RT-

qPCR was performed to evaluate the expression of the hub genes in the JBMMSCs. First, cDNA synthesis was performed under the following conditions: reverse transcription at 42 °C for 60 minutes, followed by enzyme inactivation at 70 °C for 5 minutes. The used primers are listed in **Supplementary Table 3**. The RT-qPCR reaction mixture consisted of 10 μL of $2\times$ SYBR Green Master Mix, 0.5 μL each of the forward and reverse primers (10 μM), 2 μL of cDNA template, and nuclease-free water to a final volume of 20 μL. SYBR Green chemistry was employed to detect transcripts. The reactions were performed on a QuantStudio3 Real-Time PCR System (Applied Biosystems). The thermal cycling conditions used for qPCR were as follows: initial denaturation at 95 °C for 10 minutes, followed by 40 cycles of denaturation at 95 °C for 15 seconds, and annealing/extension at 60 °C for 60 seconds. *GAPDH* was used as the endogenous control gene against which gene expression levels were normalized. All reactions were performed in triplicate to ensure reproducibility and reliability of the data. The protein levels of TNF-α, IL-1β, and IL-6 were determined by ELISA, using the following kits obtained from Elabscience (Wuhan, Hubei, China): rat TNF (E-EL-R2856c), rat IL-1β (E-EL-R0012c), and rat IL-6 (E-EL-R0015c). The mandibular tissues of rats were fixed, paraffin-embedded, and sliced for preservation. The protein expression levels of hub genes in these tissues were compared by Ysubg immunohistochemical staining using the following Huabio antibodies: EGFR (1:100, 0407-21), TGFB1 (1:200, HA721143), IL-6 (1:100, R1412-2), IL-1β (1:100, HA601036), and TNF (1:200, ER65189). Antibodies for the analysis of P53 (1:500, YT3528) and ESR1 (1:500, PT0632R) expression were purchased from Immunoway (Hangzhou, Zhejiang, China).

2.12 Statistical Analysis

Statistical analysis was performed using R software (v4.3.0, R Foundation for Statistical Computing, Vienna, Austria) for bioinformatics and GraphPad Prism (v9.0.0.121, GraphPad Software (Dotmatics) Boston, MA, USA) for experimental data. Enrichment analyses (GO and KEGG) were conducted using the clusterProfiler package 4.2 (Guangzhou Medical University, Guangzhou, Guangdong, China), with significance defined as p.adjust < 0.05 and FDR <0.05 (Benjamini–Hochberg correction).

Data from at least three independent experiments were expressed as the mean $\pm$ standard deviation. For comparisons of multiple groups (NC, ORNJ, and ORNJ + LbGP), one-way analysis of variance (ANOVA) was applied, followed by Tukey's post-hoc test. Differences with a p-value < 0.05 were considered statistically significant. This statistical approach was used to analyze data obtained by RT-qPCR, ELISA, and immunohistochemistry.

3. Results

3.1 Study Design

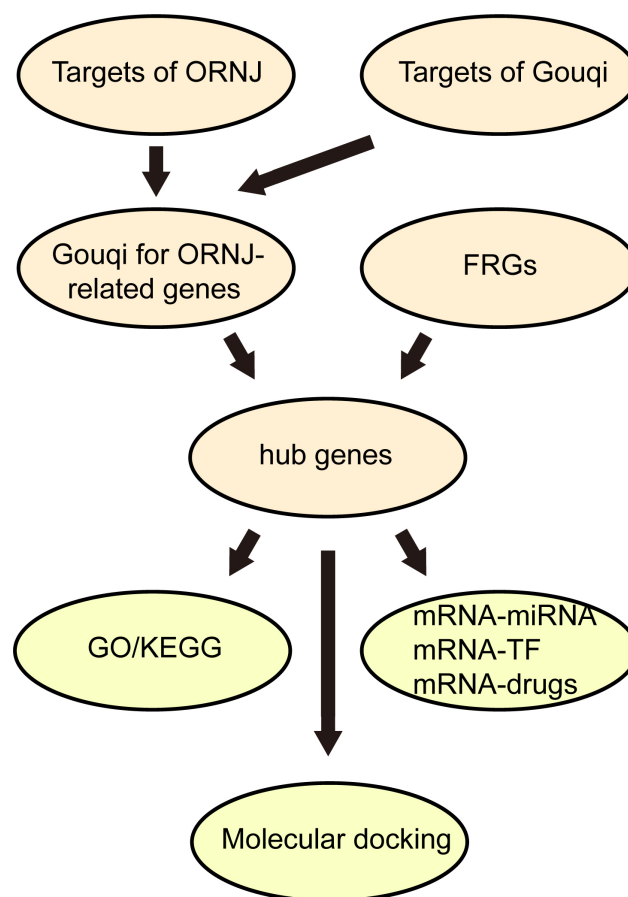The flowchart for this study is shown in Fig. 1.

Fig. 1. Technology roadmap. ORNJ, osteoradionecrosis of the jaw; FRGs, ferroptosis-related genes; GO, Gene Ontology; KEGG, Kyoto Encyclopedia of Genes and Genomes; TF, transcription factors.

3.2 Screening for Lycium barbarum-Related Genes in ORNJ Therapy

A total of 188 chemical components from *Lycium barbarum* were extracted from the TCMSP database. Among these, 45 active compounds were selected through screening for values of OB $>30\%$ and DL >0.18. Detailed data for these compounds are shown in Table 1. Protein targets for the active compounds in *Lycium barbarum* were predicted using the TCMSP database. The targets were then translated into gene names using UniProtKB, yielding a total of 205 targets for the *Lycium barbarum* constituents. The component–target network diagram is shown in Fig. 2A, and specific target information is provided in **Supplementary Table 4**.

The intersection of 205 potential target points for *Lycium barbarum* components and 35 disease target points

Table 1. Chemical constituents and ADME parameters for *Lycium barbarum*.

MOL_ID	Compound	OB (%)	DL
MOL001323	Sitosterol alpha1	43.28127042	0.78354
MOL003578	Cycloartenol	38.68565906	0.78093
MOL001494	Mandenol	41.99620045	0.19321
MOL001495	Ethyl linolenate	46.10096327	0.19716
MOL001979	LAN	42.11918897	0.74787
MOL000449	Stigmasterol	43.82985158	0.75665
MOL000358	Beta-sitosterol	36.91390583	0.75123
MOL005406	Atropine	45.97058178	0.19328
MOL005438	Campesterol	37.57681789	0.71488
MOL006209	Cyanin	47.42092269	0.75918
MOL007449	24-methylidenelophenol	44.19264545	0.75330
MOL008173	Daucosterol_qt	36.91390583	0.75316
MOL008400	Glycitein	50.47891366	0.23826
MOL010234	Delta-carotene	31.80094312	0.54639
MOL000953	CLR	37.87389754	0.67677
MOL009604	14b-pregnane	34.77923299	0.33723
MOL009612	Alpha (r)-4-methyl-24-ethylcholesta-7,25-dien-3beta-ylacetate	46.35749925	0.83980
MOL009615	24-methylenecycloartan-3beta,21-diol	37.31728162	0.79751
MOL009617	24-ethylcholest-22-enol	37.09454086	0.75110
MOL009618	24-ethylcholesta- 5,22-dienol	43.82985158	0.75636
MOL009620	24-methyl-31-norlanost-9(11)-enol	37.99968530	0.75092
MOL009621	24-methylenelanost-8-enol	42.36819868	0.76769
MOL009622	Fucosterol	43.77639556	0.75668
MOL009631	31-norcyclolaudenol	38.68209614	0.81391
MOL009633	31-norlanost-9(11)-enol	38.35394137	0.72490
MOL009634	31-norlanosterol	42.20462055	0.73012
MOL009635	4,24-methyllophenol	37.83467433	0.74999
MOL009639	Lophenol	38.12940252	0.71400
MOL009640	4alpha,14 alpha,24-trimethylcholesta-8,24-dienol	38.90988973	0.75772
MOL009641	4alpha,24-dimethylcholesta-7,24-dienol	42.65304098	0.75297
MOL009642	Alpha4-methyl-24-ethylcholesta-7,24-dienol	42.29509453	0.78304
MOL009644	6-fluoroindole-7-dehydrocholesterol	43.72602513	0.72224
MOL009646	7-O-methylluteolin-6-C-beta-glucoside_qt	40.77368843	0.30497
MOL009650	Atropine	42.15897078	0.19299
MOL009651	Cryptoxanthin monoepoxide	46.95371937	0.56103
MOL009653	Cycloeucalenol	39.72647216	0.79446
MOL009656	(E,E)-1-ethyl octadeca-3,13-dienoate	41.99620045	0.19364
MOL009660	Methyl (1R,4aS,7R,7aS)-4a,7-dihydroxy-7-methyl-1-[(2S,3R,4S,5S,6R)-3,4,5-trihydroxy-6-(hydroxymethyl)oxan-2-yl]oxy-1,5,6,7a-tetrahydrocyclopenta[d]pyran-4-carboxylate	39.42847682	0.46558
MOL009662	Lantadene A	38.67942417	0.57405
MOL009664	Physalin A	91.70647491	0.27207
MOL009665	Physcion-8-O-beta-D-gentiobioside	43.90358656	0.62426
MOL009677	lanost-8-en-3beta-ol	34.22630373	0.74036
MOL009678	Lanost-8-enol	34.22630373	0.74167
MOL009681	Obtusifoliol	42.55200222	0.75650
MOL000098	Quercetin	46.43334812	0.27525

ADME, Absorption, Distribution, Metabolism, Excretion; OB, oral bioavailability; DL, drug-likeness; LAN, Number of Liked Approved drug Analoques; CLR, Clearance.

was plotted in a Venn diagram (Fig. 2B). This yielded 11 potential *Lycium barbarum*, in traditional Chinese medicine formulation, treatment targets for ORNJ: RUNX2 (Runt-Related Transcription Factor 2), TGFB1 (Transforming Growth Factor Beta 1), TP53 (Tumor Protein p53), TNF (Tumor Necrosis Factor), IL-6 (Interleukin-6), VEGFA (Vascular Endothelial Growth Factor A), ESR1 (Estrogen Receptor 1), SPP1 (Secreted Phosphoprotein 1), IL-1β (Interleukin-1 Beta), CXCL8 (C-X-C Motif Chemokine Ligand 8), and EGFR (Epidermal Growth Factor Receptor). A component-target-pathway network was constructed (Fig. 2C).

3.3 FRGs Related to Lycium barbarum in the Treatment of Radiation-Induced Osteonecrosis of the Jaw

Seven intersection genes (*TP53*, *EGFR*, *TGFB1*, *IL-6*, *IL1B*, *TNF*, *ESR1*) were obtained from the intersection of FRGs and *Lycium barbarum* treatment ORNJRGs. These intersection genes were deemed as hub genes in the Venn diagram (Fig. 3A). Protein–protein interactions were examined in terms of the seven hub genes, resulting in the creation of a protein–protein interaction network (Fig. 3B), visualized through Cytoscape (Fig. 3C). Furthermore, for each of the seven hub genes, an interaction network of functionally related genes was predicted and built using the GeneMANIA website (Fig. 3D). This allowed the physical interactions, shared protein domains, gene interactions, and other relevant information for the hub genes to be observed.

3.4 GO and KEGG Enrichment Analysis of Hub Genes

The BP, MF, CC (Cellular Component), and biological pathways were analyzed for the seven hub genes (*TP53*, *EGFR*, *TGFB1*, *IL-6*, *IL1B*, *TNF*, *ESR1*). The results of the enrichment analysis are presented as bar graphs (Fig. 4A–C). Furthermore, the correlations between hub genes, GO results (Fig. 4D,E), and KEGG (Fig. 4F) enrichment analyses are presented as a circular network diagram.

As shown in Fig. 4A–F, the hub genes were mainly enriched in regulating the generation of miRNAs involved in gene silencing through microRNAs, small RNA generation involved in gene silencing through RNA, miRNA-mediated gene silencing, gene silencing through RNA, post-transcriptional gene silencing, post-transcriptional gene silencing through RNA, miRNA generation involved in gene silencing through miRNA, primary sncRNA processing, and the negative and positive regulation of the generation of miRNAs involved in gene silencing through miRNA. The regulation of other BPs included cytokine receptor binding, signaling receptor activator activity, cytokine activity, receptor ligand activity, RNA polymerase II common transcription initiation factor binding, common transcription initiation factor binding, basal transcription machinery binding, basal RNA polymerase II transcription machinery binding, and ATPase binding, as well as MFs such as protease binding. The hub genes were mainly en-

riched in malaria, inflammatory bowel disease, cancer proteoglycans, cytomegalovirus infection, rheumatoid arthritis, the Advanced Glycation End-products-Receptor for Advanced Glycation End-products (AGE-RAGE) signaling pathway in diabetic complications, Chagas disease, Amoebiasis, the MAPK signaling pathway, and antifolate resistance pathway (Table 2).

3.5 Networks for mRNA–miRNA, mRNA–TF, and mRNA–drug Interactions

The mRNA–miRNA data identified miRNAs that interact with the seven hub genes (*TP53*, *EGFR*, *TGFB1*, *IL-6*, *IL1B*, *TNF*, and *ESR1*). A visual representation of the mRNA–miRNA interaction network was created using the Cytoscape software (Fig. 5A). Six hub genes (*TP53*, *EGFR*, *TGFB1*, *IL-6*, *IL1B*, *ESR1*) and 73 miRNA molecules were included in this network, yielding 129 pairs of interactions between mRNA and miRNA. Detailed information on these interactions is shown in **Supplementary Table 5**.

We next searched the CHIPBase database for TFs that interact with the hub genes. Interaction information was extracted from the two databases and intersected with the seven hub genes, thereby demonstrating interactions between the seven hub genes and 81 TFs, as visualized using Cytoscape (Fig. 5B). Details of the mRNA–TF interactions are shown in **Supplementary Table 6**.

Possible medications or chemical compounds for the seven hub genes were identified using the CTD database. The mRNA–drug interaction network (Fig. 5C) revealed 73 possible pharmaceuticals or chemical substances that interact with six hub genes (*TP53*, *TGFB1*, *IL-6*, *IL1B*, *TNF*, *ESR1*) (**Supplementary Table 7**).

3.6 Docking Analysis of Hub Genes and Core Active Components

Based on the disease target–Lycium active ingredient–pathway network shown in Fig. 2C, three active ingredients related to the seven hub genes were identified: β-sitosterol (MOL000358), glycitein (MOL008400), and quercetin (MOL000098). By using Autodock Vina for the molecular docking of hub genes with core active ingredients and then selecting optimal conformations, eight protein–active ingredient docking structures were obtained, all with binding free energies $<$–5 kcal/mol (Table 3). Molecular interactions for the eight binding conformations were subsequently analyzed using PLIP and visualized with PyMOL (Fig. 6A–H). From the docking results and a molecular mechanics perspective, TGFB1 was capable of forming hydrogen bonds with the Lycium β-sitosterol component, generating hydrophobic forces (Fig. 6A). ESR1 was able to form hydrogen bonds with the Lycium glycitein component, generating hydrophobic forces (Fig. 6B). EGFR was capable of forming hydrogen bonds with the Lycium quercetin component, generating hydrophobic forces (Fig. 6C). TNF could form hydrogen bonds with the Lycium quercetin compo-
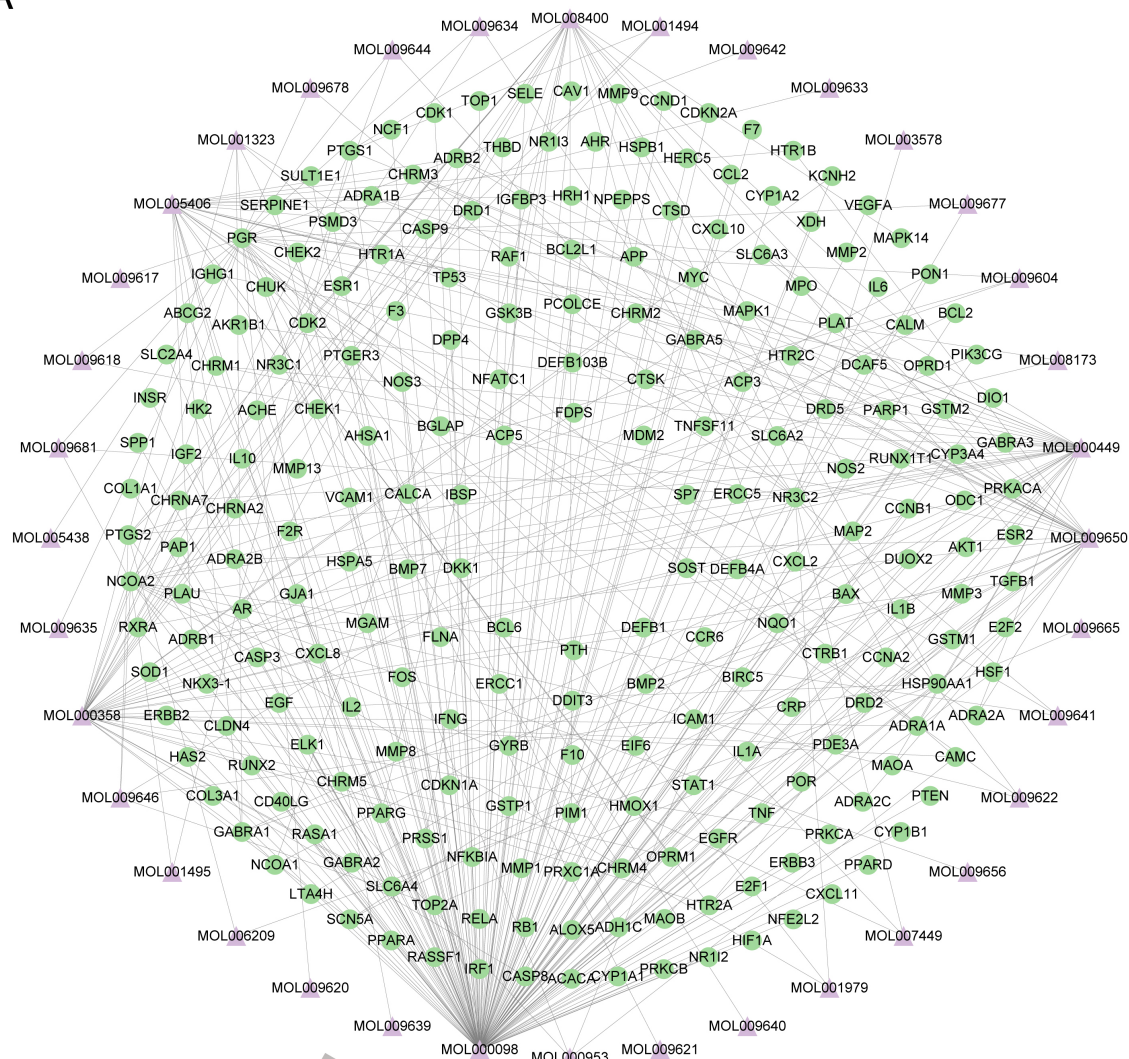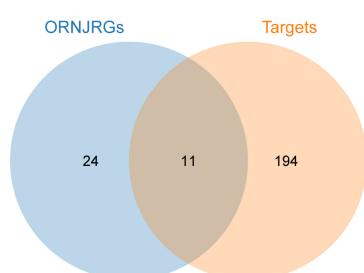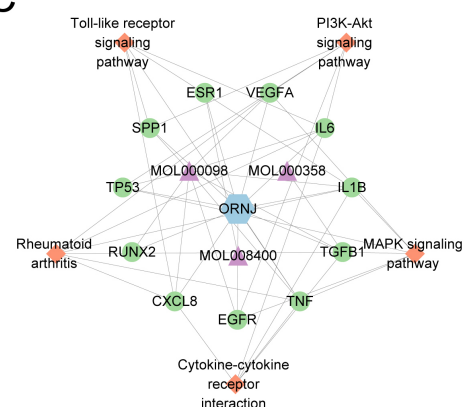
Fig. 2. Target screening for *Lycium barbarum* and ORNJ. (A) Network diagram of predicted targets of active chemical constituents in Lycium barbarum. (B) Venn diagram of the predicted targets of active components in *Lycium barbarum* and ORNJ-related genes. (C) Active chemical components, ORNJ-related genes, and the KEGG pathway network map for Lycium barbarum. ORNJ, osteoradionecrosis of the jaw; ORNJRGs, osteoradionecrosis of the jaw related genes; KEGG, Kyoto Encyclopedia of Genes and Genomes. In panels (A) and (C), the green circles represent mRNAs, purple triangles are chemical components, blue hexagons are ORNJ, and orange quadrangles are the KEGG pathways.
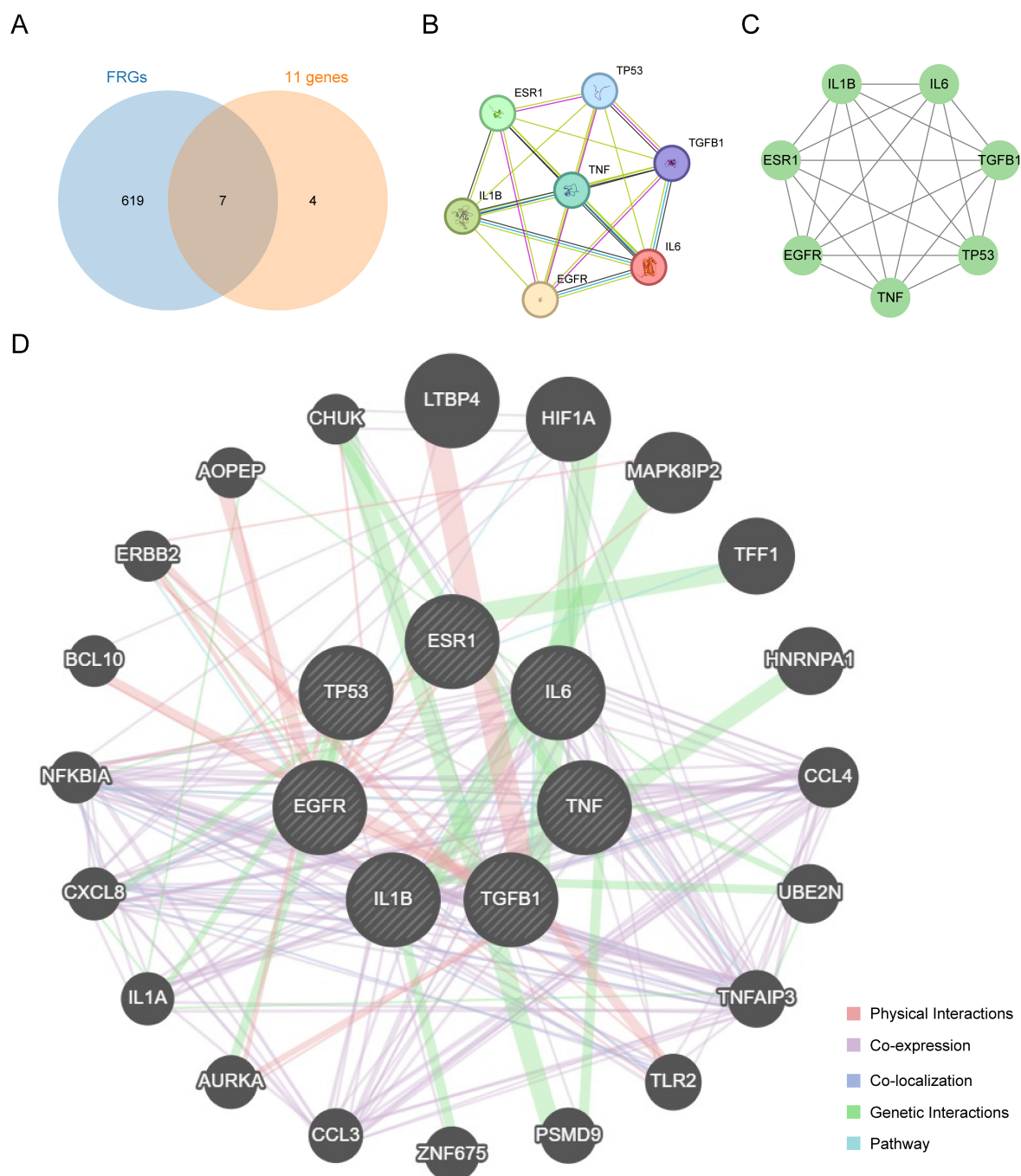
Fig. 3. Protein–protein interaction network. (A) Intersection Venn diagram of ferroptosis-related genes and 11 genes related to *Lycium barbarum* treatment of radiation-induced osteonecrosis of the jaw. (B) Protein interaction network diagram obtained from the STRING database. (C) Protein interaction network drawn by Cytoscape. (D) Interaction network of functionally similar genes of hub genes on the GeneMANIA website. In this network, black circles with white slash lines represent input hub genes, while other black circles without white slash lines represent predicted functionally similar genes.

nent, generating hydrophobic forces (Fig. 6D). IL-6 was able to form hydrogen bonds with the Lycium quercetin component, generating hydrophobic forces (Fig. 6E). TP53 was capable of forming hydrogen bonds with the Lycium quercetin component, generating hydrophobic forces (Fig. 6F). IL-1β was able to form hydrogen bonds with Lycium quercetin component, generating hydrophobic forces

(Fig. 6G). Finally, TGFB1 could form hydrogen bonds with the Lycium quercetin component, generating hydrophobic forces (Fig. 6H).

3.7 Validation of the Results

We next investigated the therapeutic effects of LbGP on ORNJ. The RT-qPCR data showed that the mRNA lev-
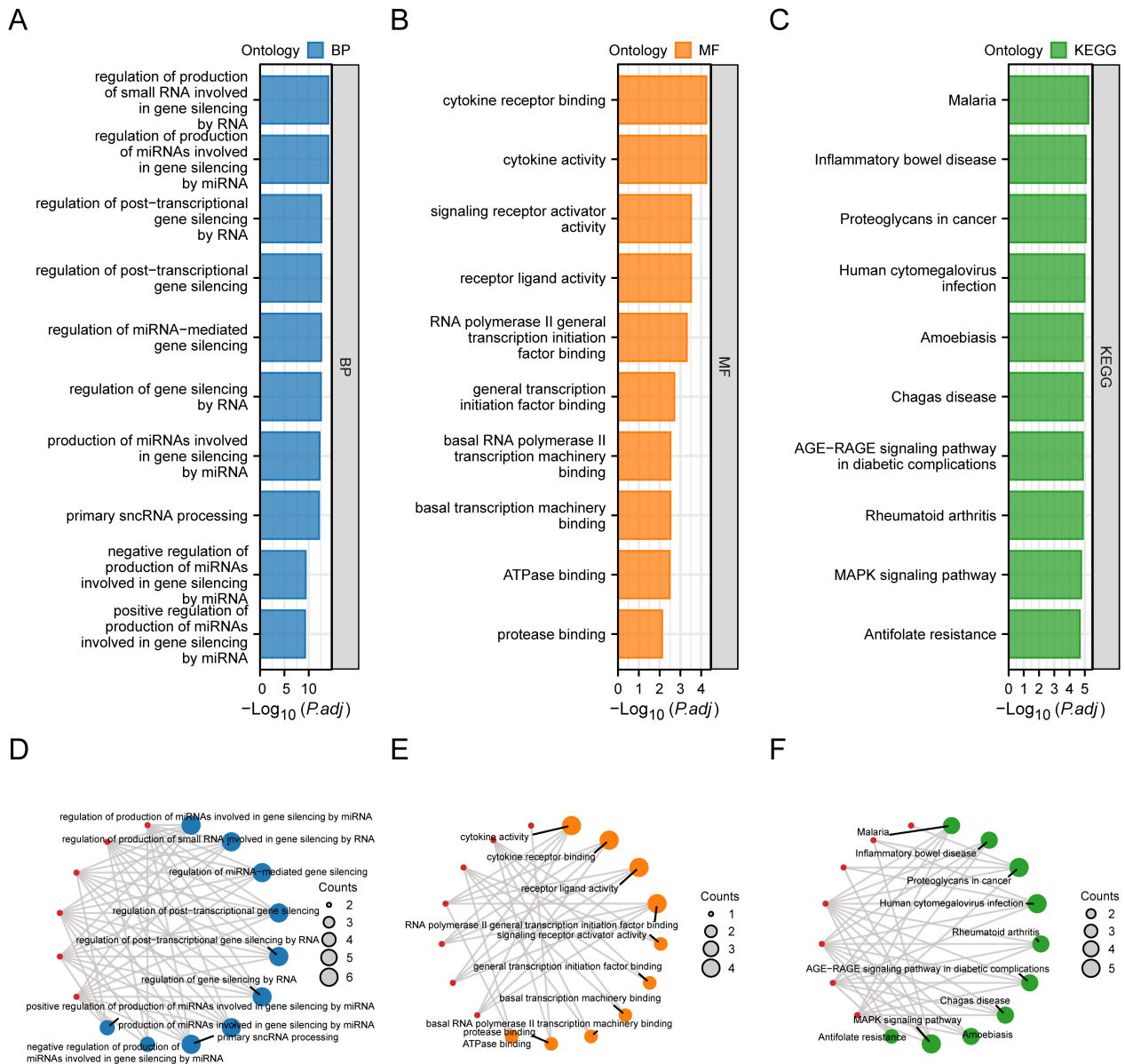
Fig. 4. Functional enrichment analysis (GO) and pathway enrichment (KEGG) analysis of hub genes. (A) Bar graph of the results of BP functional enrichment analysis of hub genes. (B) Ring bar chart of MF functional enrichment analysis results of hub genes. (C) Bar chart of KEGG pathway enrichment analysis results of hub genes. (D) Network diagram of BP functional enrichment analysis results of hub genes. (E) Ring network diagram of MF functional enrichment analysis results of hub genes. (F) Network diagram of KEGG pathway enrichment analysis results of hub genes. GO, Gene Ontology; BP, biological process; MF, molecular function; KEGG, Kyoto Encyclopedia of Genes and Genomes. (D–F): the blue circles are used to denote the BP entries, orange circles for MF entries, green circles for KEGG entries, and red circles for genes.

els of *IL1B* and *IL-6* were significantly reduced in rat JB-MMSCs treated with LbGP compared to the ORNJ group; however, the levels of these mRNAs remained higher than in the NC group. The mRNA levels of *TP53* and *TNF* were also lower in the LbGP group, whereas those of *EGFR* and *TGFB1* increased. The mRNA level of *ESR1* showed no significant change (Fig. 7A). The ELISA results exhibited significantly decreased protein levels of TNF-α, IL-1β, and

IL-6 in the cell culture supernatant of the LbGP treatment group compared to the ORNJ group (Fig. 7B). Immunohistochemical analysis also showed significantly reduced positivity for P53, TGFβ1, IL-6, and TNF in the *Lycium barbarum* peptide extract group compared to the ORNJ group. Positive staining for EGF was increased, while there were no obvious changes in positive staining for IL-1β and ESR1 (Fig. 7C). Therefore, LbGP may alleviate ORNJ-induced

Table 2. GO and KEGG enrichment analysis results of hub genes.

ID	Description	GeneRatio	BgRatio	p-value	p.adjust	q-value
GO:1903798	Regulation of the production of miR-NAs involved in gene silencing by miRNA	6/7	22/18,800	8.51780×10^{-18}	9.56455×10^{-15}	1.49200×10^{-15}
GO:0070920	Regulation of the production of small RNAs involved in gene silencing by RNA	6/7	23/18,800	1.15236×10^{-17}	9.56455×10^{-15}	1.49200×10^{-15}
GO:0060964	Regulation of miRNA-mediated gene silencing	6/7	42/18,800	5.98311×10^{-16}	2.67277×10^{-13}	4.16931×10^{-14}
GO:0060147	Regulation of post-transcriptional gene silencing	6/7	44/18,800	8.05050×10^{-16}	2.67277×10^{-13}	4.16931×10^{-14}
GO:1900368	Regulation of post-transcriptional gene silencing by RNA	6/7	44/18,800	8.05050×10^{-16}	2.67277×10^{-13}	4.16931×10^{-14}
GO:0060966	Regulation of gene silencing by RNA	6/7	46/18,800	1.06814×10^{-15}	2.95519×10^{-13}	4.60988×10^{-14}
GO:0035196	Production of miRNAs involved in gene silencing by miRNA	6/7	52/18,800	2.32094×10^{-15}	5.50395×10^{-13}	8.58574×10^{-14}
GO:0070918	Primary sncRNA processing	6/7	56/18,800	3.70084×10^{-15}	7.67924×10^{-13}	1.19790×10^{-13}
GO:1903799	Negative regulation of the production of miRNAs involved in gene silencing by miRNA	4/7	11/18,800	2.21775×10^{-12}	4.09051×10^{-10}	6.38089×10^{-11}
GO:1903800	Positive regulation of the production of miRNAs involved in gene silencing by miRNA	4/7	12/18,800	3.32620×10^{-12}	5.52149×10^{-10}	8.61310×10^{-11}
GO:0005125	Cytokine activity	4/7	235/18,410	8.78981×10^{-7}	5.67143×10^{-5}	1.16082×10^{-5}
GO:0005126	Cytokine receptor binding	4/7	272/18,410	1.57540×10^{-6}	5.67143×10^{-5}	1.16082×10^{-5}
GO:0048018	Receptor ligand activity	4/7	489/18,410	1.61493×10^{-5}	0.00030746	6.29304×10^{-5}
GO:0030546	Signaling receptor activator activity	4/7	496/18,410	1.70811×10^{-5}	0.00030746	6.29304×10^{-5}
GO:0001091	RNA polymerase II general transcription initiation factor binding	2/7	24/18,410	3.40678×10^{-5}	0.000490576	0.00010041
GO:0140296	General transcription initiation factor binding	2/7	52/18,410	0.000162845	0.001954141	0.00039997
GO:0001098	Basal transcription machinery binding	2/7	74/18,410	0.000330387	0.002973487	0.000608608
GO:0001099	Basal RNA polymerase II transcription machinery binding	2/7	74/18,410	0.000330387	0.002973487	0.000608608
GO:0051117	ATPase binding	2/7	82/18,410	0.000405637	0.003245097	0.000664201
GO:0002020	Protease binding	2/7	136/18,410	0.001110341	0.007588935	0.001553291
hsa05144	Malaria	4/7	50/8164	4.29924×10^{-8}	5.84697×10^{-6}	1.94597×10^{-6}
hsa05321	Inflammatory bowel disease	4/7	65/8164	1.25831×10^{-7}	8.55649×10^{-6}	2.84775×10^{-6}
hsa05205	Proteoglycans in cancer	5/7	205/8164	1.91753×10^{-7}	8.69279×10^{-6}	2.89311×10^{-6}
hsa05163	Human cytomegalovirus infection	5/7	225/8164	3.05480×10^{-7}	1.03863×10^{-5}	3.45675×10^{-6}
hsa05323	Rheumatoid arthritis	4/7	93/8164	5.38164×10^{-7}	1.32803×10^{-5}	4.41990×10^{-6}
hsa04933	AGE-RAGE signaling pathway in diabetic complications	4/7	100/8164	7.21259×10^{-7}	1.32803×10^{-5}	4.41990×10^{-6}
hsa05142	Chagas disease	4/7	102/8164	7.81191×10^{-7}	1.32803×10^{-5}	4.41990×10^{-6}
hsa05146	Amoebiasis	4/7	102/8164	7.81191×10^{-7}	1.32803×10^{-5}	4.41990×10^{-6}
hsa04010	MAPK signaling pathway	5/7	294/8164	1.15907×10^{-6}	1.75149×10^{-5}	5.82925×10^{-6}
hsa01523	Antifolate resistance	3/7	30/8164	1.55196×10^{-6}	2.11067×10^{-5}	7.02466×10^{-6}

GO, Gene Ontology; KEGG, Kyoto Encyclopedia of Genes and Genomes; MAPK, Mitogen-Activated Protein Kinase.

tissue injury in rats by regulating the mRNA expression levels of *TP53*, *EGFR*, *IL-6*, and *TNF* and of the corresponding translated proteins.

4. Discussion

The incidence of osteoradionecrosis among patients receiving radiotherapy for head and neck malignancies ranges from 0% to 23%, representing a serious compli-
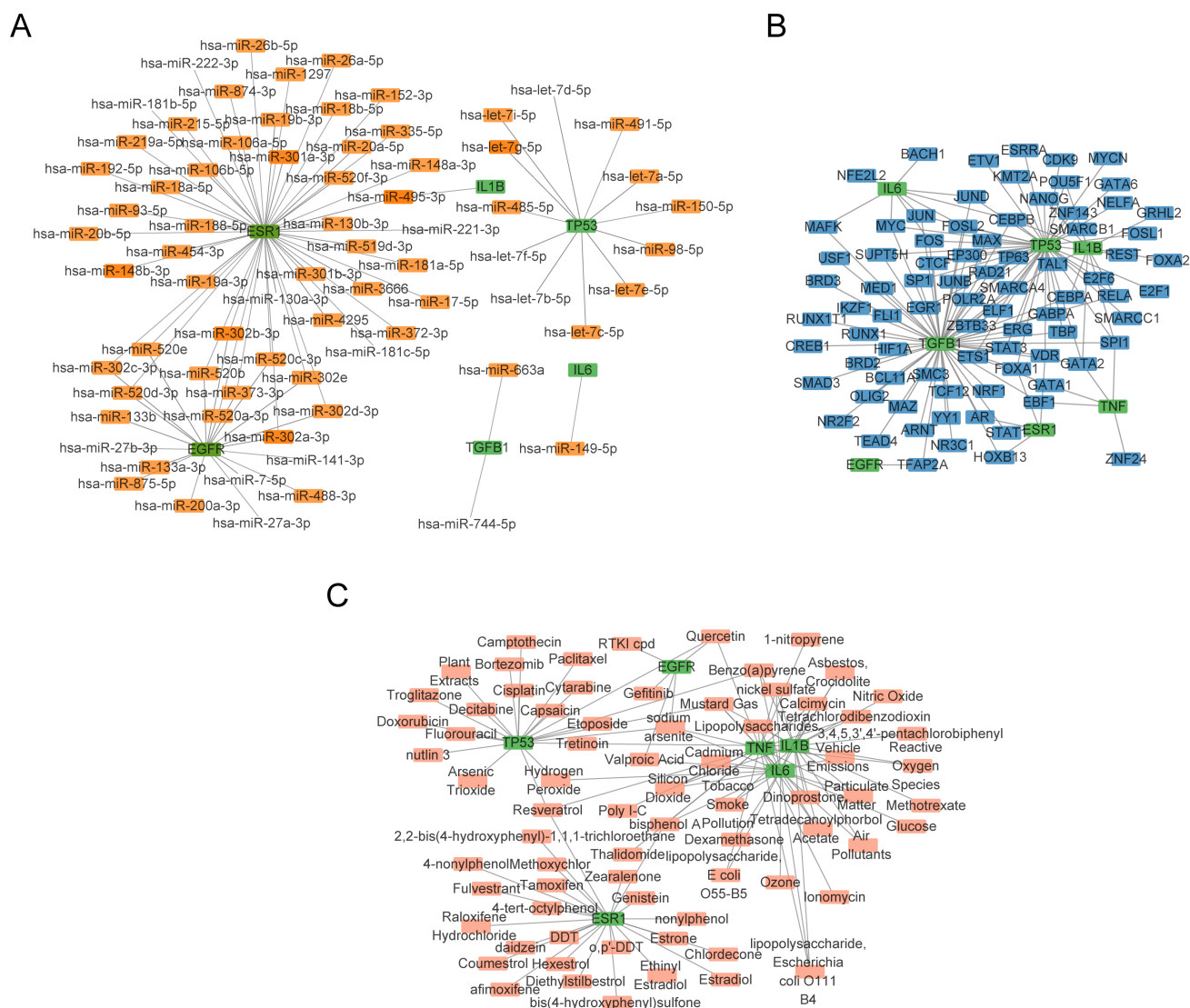
Fig. 5. Construction of mRNA–miRNA, mRNA–TF, and mRNA–drug interaction networks. (A–C) mRNA–miRNA (A), mRNA–TF (B), mRNA–drug (C) interaction networks of hub genes. Green squares are mRNAs; orange squares are miRNAs; blue squares are TFs; pink squares are small-molecule drugs. TFs, transcription factors.

Table 3. Molecular docking binding energy (kcal/mol).

Gene	Compound	Binding energy
TGFB1	Beta-sitosterol	6.0
ESR1	Glycitein	7.1
EGFR	Quercetin	8.6
TNF	Quercetin	6.8
IL-6	Quercetin	7.0
TP53	Quercetin	5.8
IL1B	Quercetin	6.3
TGFB1	Quercetin	6.5

cation of the applied treatment. Meanwhile, a higher prevalence is observed among older and male patients [1]. Following radiotherapy, most patients experience reduced salivary secretion, increased susceptibility to rampant caries, secondary odontogenic infections, and pro-longed non-healing wounds resulting from extractions or other injuries. The latter occasionally leads to fistula formation with minimal purulent discharge, accompanied by persistent pain and halitosis. Occasionally, soft tissue may undergo necrosis and ulceration, exposing necrotic bone that is non-mobile, leading to a chronic inflammatory process that significantly impacts the quality of life and oral health of the patients. Currently, treatment modalities for osteoradionecrosis mainly comprise oral antibiotics, oral hygiene measures, surgical interventions, and hyperbaric oxygen therapy. However, existing treatment modalities have limitations, such as relying solely on medications and local wound care. Although partially effective, this may overestimate clinical resolution due to the inclusion of so-called "mild" cases of osteoradionecrosis. Additionally, surgical interventions entail inherent risks, while hyperbaric oxygen therapy is both expensive and laborious.
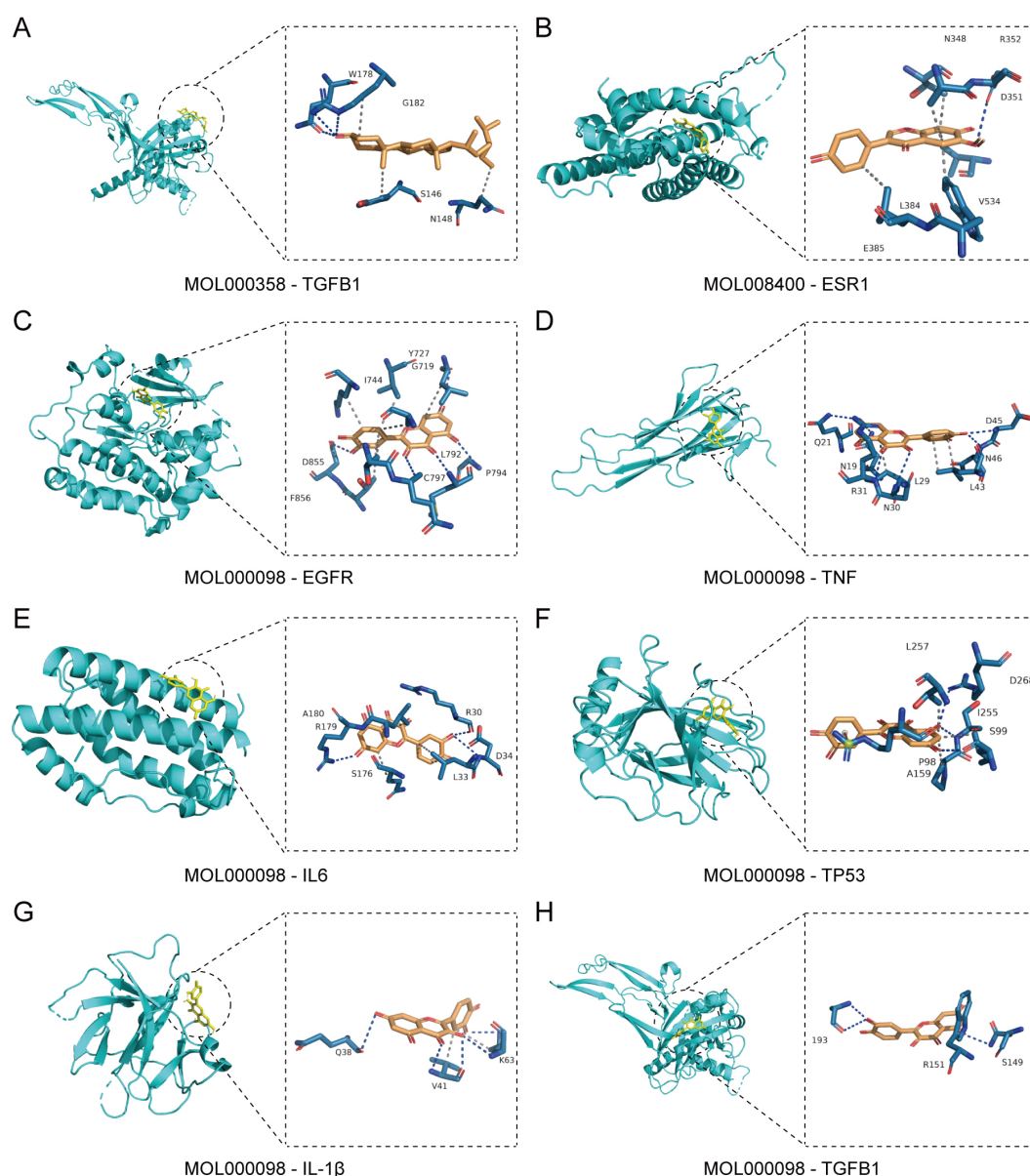
Fig. 6. Docking analysis of hub genes with core active components. (A) Mode of binding of Transforming Growth Factor Beta 1 (TGFB1) to β-sitosterol components in *Lycium barbarum*. (B) The binding mode of Estrogen Receptor 1 (ESR1) to the glycitein component in *Lycium barbarum*. (C) The binding mode of Epidermal Growth Factor Receptor (EGFR) to the quercetin component in *Lycium barbarum*. (D) Pattern of TNF binding to quercetin components in *Lycium barbarum*. (E) Binding mode of IL-6 to quercetin components in *Lycium barbarum*. (F) The binding mode of TP53 to quercetin components in *Lycium barbarum*. (G) Mode of binding of IL-1β to quercetin components in *Lycium barbarum*. (H) Mode of binding of TGFB1 to quercetin components in *Lycium barbarum*. Interaction force line: blue dashed line indicates hydrogen bonding; black dashed line indicates hydrophobic interaction. Bright blue indicates the protein structure of the hub genes, yellow and orange highlight the active components, and dark blue shows the amino acid residues that interact with the active components.

Thus, the investigation of the potential therapeutic effects of *Lycium barbarum* is of significant importance and urgency. *Lycium barbarum* possesses numerous medicinal features, including anti-inflammatory, immunomodulatory, and antioxidative properties, which can exert beneficial effects in treating osteoradionecrosis. Nevertheless, thorough studies on the effectiveness of *Lycium barbarum* and its mode of action in osteoradionecrosis remain limited. Further screening of the bioactive components of *Lycium barbarum* is needed to evaluate its feasibility and efficacy as
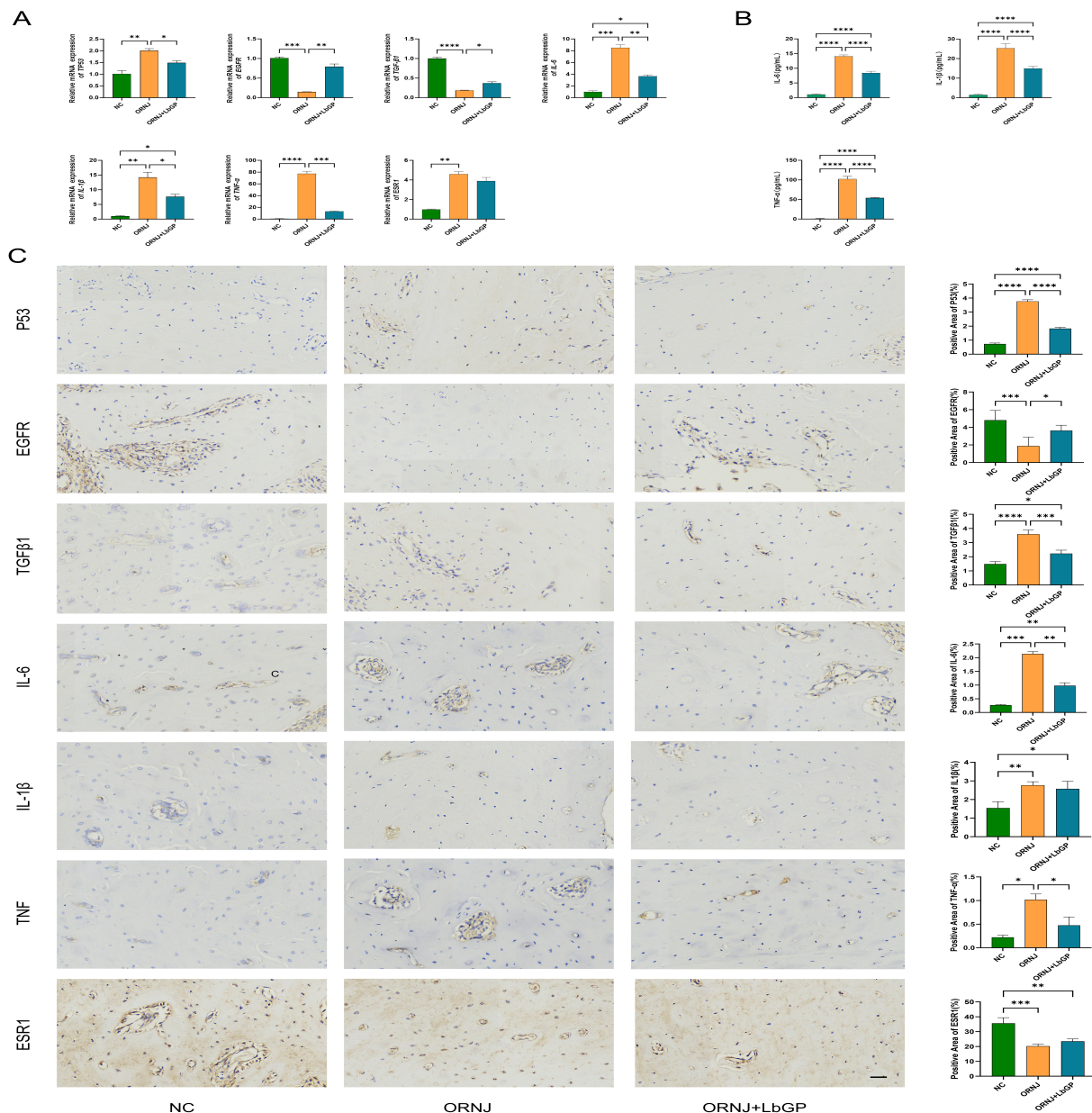
Fig. 7. RT-qPCR validation, ELISA validation, and immunohistochemical validation of paraffin-embedded sections of rat mandible tissue. (A) Relative mRNA expressions of hub genes in the normal, ORNJ, and treatment groups. (B) Protein expressions of tumor necrosis factor-alpha (TNF-α), IL-1β, and IL-6. (C) Positive area of hub gene-related proteins. Bar = 30 μm. Data are presented as the mean $\pm$ standard deviation of three independent experiments (n = 3). Statistical significance was evaluated using ANOVA. *$p <$ 0.05; **$p <$ 0.01; ***$p <$ 0.001; ****$p <$ 0.0001.

a treatment for osteoradionecrosis. This will provide a scientific basis for clinical practice and should eventually enhance treatment results and patient quality of life.

We first obtained the compositional information of *Lycium barbarum* from the TCMSP database and utilized its ADME-related characteristic data. Active constituents were screened based on the OB and DL values. Subsequently, the active ingredients were converted into gene names to predict the corresponding protein targets in Lycium barbarum. To assess the involvement of ferroptosis in

ORNJ, we identified 626 unique FRGs from the GeneCards, MSigDB, and FerrDb databases. Additionally, we identified *Lycium barbarum* treatment-related genes for ORNJ by intersecting these genes with the previously screened ORNJRGs. Subsequently, seven hub genes (*TP53*, *EGFR*, *TGFB1*, *IL-6*, *IL1B*, *TNF*, *ESR1*) were identified, allowing a corresponding protein–protein interaction analysis to establish a network.

Utilizing the disease target–*Lycium barbarum* active ingredient–pathway network, we identified three active ingredients in *Lycium barbarum* associated with the seven hub genes; notably, β-sitosterol, glycitein, and quercetin. β-sitosterol exhibits significant anti-inflammatory properties and can reduce the expression of intracellular adhesion molecule 1 and vascular adhesion molecule 1 in TNF-α-stimulated HAECs [24]. Quercetin has efficient anti-inflammatory properties [25]. Moreover, quercetin can hinder the production of TNF-α prompted by lipopolysaccharide in macrophages. Furthermore, quercetin can inhibit IL-6 secretion, as well as the IL-1-induced phosphorylation of p38 and PKC-θ (Protein Kinase C-theta). This indicates promising pharmacological effects in inflammation [26]. Glycitein exhibits antioxidant, anti-inflammatory, and hormone-regulating effects [27]. Additionally, glycitein demonstrates anti-inflammatory effects by activating various biochemical and molecular pathways that mitigate inflammatory responses, suggesting potential in preventing and treating inflammatory diseases [28]. The anti-inflammatory and immune-regulating components found in *Lycium barbarum* align with the research findings on radiation-induced osteomyelitis, a secondary infection resulting from radiation exposure.

GO and KEGG enrichment analyses were performed to identify the regulatory pathways and biological processes of key genes. Our findings suggest that *Lycium barbarum* may be involved in biological processes, including cytokine receptor binding and receptor–ligand interactions. Immune cells release a variety of cytokines in response to infection, injury, or damage, including TNF and IL-6. These cytokines trigger inflammatory responses that lead to vasodilation and increased vascular permeability, containing the spread of infection. However, excessive or prolonged inflammatory responses can be detrimental to the body. Gene expression can be modulated through the inhibition of target gene translation or through mRNA degradation. This can occur via the regulation of miRNAs, by mediating gene silencing through miRNAs, and by post-transcriptional gene silencing. The MAPK signaling pathway can be stimulated by diverse inflammatory factors [29], exerting a crucial regulatory function in the development and spread of inflammation. Investigating the influence of *Lycium barbarum* on inflammatory factors holds great potential for preventing and managing infections and inflammatory reactions. Finally, we investigated the underlying treatment effects of LbGP extract on ORNJ. Using LbGP as the intervention drug, mesenchymal stem cells from the mandible of ORNJ rats were cultured and examined by qPCR. The mRNA expression levels of *TP53*, *IL-6*, and *TNF* were observed to decrease, while the expression of *EGFR* increased. ELISA confirmed the reduced expression of IL-6 and TNF-α at the protein level. Immunohistochemical analysis of the jawbone tissues of ORNJ rats treated with LbGP further confirmed the changes in expression of P53, EGFR, IL-6, and TNF-α. The tumor suppressor gene *TP53* is involved in regulating the cell cycle and in DNA repair [30,31]. Following exposure to ionizing radiation, the expression of P53 protein increases, thereby affecting cell fate through apoptosis or changes in DNA repair mechanisms [32]. The active ingredients in LbGP may play a protective role against jawbone injury after radiation by regulating the expression of *TP53*. *EGFR* is a widely expressed receptor tyrosine kinase that is often overexpressed in tumor cells. Studies have shown that *EGFR* is a driver oncogene for advanced head and neck squamous cell carcinoma (HNSCC), as well as a therapeutic target [33,34]. The active ingredients of *Lycium barbarum* may influence the development of ORNJ, a complication of HNSCC radiotherapy, by regulating the activation of *EGFR*. *IL-6* and *TNF* are key pro-inflammatory factors involved in apoptosis, inflammation, and immune responses. Elevated expression of these cytokines may be related to the acute inflammatory response induced by radiation damage, thereby promoting the progression of osteomyelitis. The expression levels of IL-6 and TNF-α in the LbGP intervention group were significantly lower than those in the ORNJ group, further supporting the potential role of *Lycium barbarum* in regulating the local inflammatory microenvironment in ORNJ. Finally, this study is the first to investigate the regulatory effects of *Lycium barbarum* on *TP53*, *EGFR*, *IL-6*, and *TNF* in ORNJ. Our results suggest that *Lycium barbarum* may be used as a potential adjuvant treatment for ORNJ.

Although this study identified some bioactive compounds in *Lycium barbarum*, time constraints prevented us from carrying out functional experiments to demonstrate their therapeutic effects on osteoradionecrosis. The animal experiments in this study primarily focused on the expression of inflammatory factors and certain key genes. Specific indicators of ferroptosis, such as GPX4, ACSL4, and lipid peroxides, were not included in the analysis. Therefore, the role of ferroptosis is currently based on the extrapolation of bioinformatics data and indirect evidence. Secondly, the core small molecule components identified in the computational analysis were β-sitosterol, glycitein, and quercetin, whereas the actual verification in the *in vivo* animal experiments used LbGP. Some gaps were seen between the predicted and verified objects, and these did not fully correspond to the effects of specific small-molecule components. Moreover, the sample size in our animal study was limited, only one time point was used, and multi-omics systematic verification was not carried out. Therefore, the conclusions of this study should be regarded as preliminary. Further research is needed to combine specific ferroptosis-related detection, verify different active components, and conduct larger-scale systematic experiments and clinical studies. This should lead to a more comprehensive understanding of the underlying mechanism and potential clinical value of *Lycium barbarum* in ORNJ.

5. Conclusion

This study initially identified seven key hub genes (*TP53*, *EGFR*, *TGFB1*, *IL-6*, *IL1B*, *TNF*, and *ESR1*) that interact with active components of *Lycium barbarum* and may play a role in the treatment of ORNJ. The active components, identified as β-sitosterol, glycitein, and quercetin, can potentially bind effectively to the hub genes. Enrichment analysis revealed several pathways related to cytokines and miRNA-regulated genes. Eight protein-active ingredient docking structures were uncovered, shedding light on possible interactions between immune cells and *Lycium barbarum*. RT-qPCR, ELISA, and immunohistochemical analysis of rat mandibular tissue confirmed that the extract of *Lycium barbarum* may exert therapeutic effects on the mandible injury of ORNJ by regulating the expression of *TP53*, *EGFR*, *IL-6*, and *TNF*. This research suggests potential new therapeutic targets and immune-regulated therapies for bone regeneration. Future studies will focus on validating these findings in animal and human models.

Availability of Data and Materials

The datasets used and analyzed during the current study are available from the corresponding author on reasonable request. Data are available in a public, open access repository, Data are available on reasonable request. This study also utilized data from the following publicly available resources: TCMSP (https://tcmsp-e.com/tcmsp.php), GeneCards (https://www.genecards.org/), MSigDB (https://www.gsea-msigdb.org/gsea/msigdb/), FerrDb (http://www.zhounan.org/ferrdb/current/), STRING (https://cn.string-db.org), KEGG (https://www.kegg.jp), ENCORI (https://rnasysu.com/encori/), CHIPBase (https://rna.sysu.edu.cn/chipbase/), CTD (https://ctdbase.org/), and RCSB PDB (https://www.rcsb.org).

Author Contributions

Conceptualization and design of the study were conducted by LF and YM. Data analysis and interpretation were performed by LF, JW, ZW, LS and LZ. LF, JW and LZ wrote manuscript. YM, JW, LS and LZ revised the manuscript. All authors contributed to editorial changes in the manuscript. All authors read and approved the final manuscript. All authors have participated sufficiently in the work and agreed to be accountable for all aspects of the work.

Ethics Approval and Consent to Participate

This study complies with international and national ethical guidelines, and follows the ARRIVE (Animal Research: Reporting *In Vivo* Experiments) guidelines. Approval for the animal experiments was obtained from the appropriate Institutional Animal Care and Use Committee (Ethics Committee of Sichuan Provincial People's Hospital), with approval number 2021 No. 336.

Conflict of Interest

The authors declare no conflict of interest.

Supplementary Material

Supplementary material associated with this article can be found, in the online version, at https://doi.org/10.31083/IJP44912.

References

[1] Kovarik PDE, Patil R, Cvek J, Kelly C, Jackson M, Mackenzie L, *et al*. Extra-mandibular Osteoradionecrosis after the Treatment of Head and Neck Cancer. Clinical Oncology (Royal College of Radiologists (Great Britain)). 2023; 35: e498–e505. https://doi.org/10.1016/j.clon.2023.06.013.

[2] Topkan E, Kucuk A, Somay E, Yilmaz B, Pehlivan B, Selek U. Review of Osteoradionecrosis of the Jaw: Radiotherapy Modality, Technique, and Dose as Risk Factors. Journal of Clinical Medicine. 2023; 12: 3025. https://doi.org/10.3390/jcm12083025.

[3] Frankart AJ, Frankart MJ, Cervenka B, Tang AL, Krishnan DG, Takiar V. Osteoradionecrosis: Exposing the Evidence Not the Bone. International Journal of Radiation Oncology, Biology, Physics. 2021; 109: 1206–1218. https://doi.org/10.1016/j.ijrobp.2020.12.043.

[4] Huang N, Wang P, Gong P, Huang B. The Progress in Reconstruction of Mandibular Defect Caused by Osteoradionecrosis. Journal of Oncology. 2023; 2023: 1440889. https://doi.org/10.1155/2023/1440889.

[5] Lei G, Zhang Y, Koppula P, Liu X, Zhang J, Lin SH, *et al*. The role of ferroptosis in ionizing radiation-induced cell death and tumor suppression. Cell Research. 2020; 30: 146–162. https://doi.org/10.1038/s41422-019-0263-3.

[6] Jiang SJ, Xiao X, Li J, Mu Y. Lycium barbarum polysaccharide-glycoprotein ameliorates ionizing radiation-induced epithelial injury by regulating oxidative stress and ferroptosis via the Nrf2 pathway. Free Radical Biology & Medicine. 2023; 204: 84–94. https://doi.org/10.1016/j.freeradbiomed.2023.04.020.

[7] Zhao L, Zhang H, Li N, Chen J, Xu H, Wang Y, *et al*. Network pharmacology, a promising approach to reveal the pharmacology mechanism of Chinese medicine formula. Journal of Ethnopharmacology. 2023; 309: 116306. https://doi.org/10.1016/j.jep.2023.116306.

[8] Lai Y, Zhong XB. Special Section on Pharmacokinetics and ADME of Biological Therapeutics-Editorial. Drug Metabolism And Disposition. 2022; 50: 819–821. https://dx.doi.org/10.1124/dmd.122.000896.

[9] Boutet E, Lieberherr D, Tognolli M, Schneider M, Bairoch A. UniProtKB/Swiss-Prot. Methods in Molecular Biology

(Clifton, N.J.). 2007; 406: 89–112. https://doi.org/10.1007/978-1-59745-535-0_4.

[10] Stelzer G, Rosen N, Plaschkes I, Zimmerman S, Twik M, Fishilevich S, *et al*. The GeneCards Suite: From Gene Data Mining to Disease Genome Sequence Analyses. Current Protocols in Bioinformatics. 2016; 54: 1.30.1–1.30.33. https://doi.org/10.1002/cpbi.5.

[11] Liberzon A, Birger C, Thorvaldsdóttir H, Ghandi M, Mesirov JP, Tamayo P. The Molecular Signatures Database (MSigDB) hallmark gene set collection. Cell Systems. 2015; 1: 417–425. https://doi.org/10.1016/j.cels.2015.12.004.

[12] Zhou N, Bao J. FerrDb: a manually curated resource for regulators and markers of ferroptosis and ferroptosis-disease associations. Database: the Journal of Biological Databases and Curation. 2020; 2020: baaa021. https://doi.org/10.1093/database/baaa021.

[13] Szklarczyk D, Gable AL, Lyon D, Junge A, Wyder S, Huerta-Cepas J, *et al*. STRING v11: protein-protein association networks with increased coverage, supporting functional discovery in genome-wide experimental datasets. Nucleic Acids Research. 2019; 47: D607–D613. https://doi.org/10.1093/nar/gky1131.

[14] Kanehisa M, Goto S. KEGG: kyoto encyclopedia of genes and genomes. Nucleic Acids Research. 2000; 28: 27–30. https://doi.org/10.1093/nar/28.1.27.

[15] Yu G, Wang LG, Han Y, He QY. clusterProfiler: an R package for comparing biological themes among gene clusters. Omics: a Journal of Integrative Biology. 2012; 16: 284–287. https://doi.org/10.1089/omi.2011.0118.

[16] Li JH, Liu S, Zhou H, Qu LH, Yang JH. starBase v2.0: decoding miRNA-ceRNA, miRNA-ncRNA and protein-RNA interaction networks from large-scale CLIP-Seq data. Nucleic Acids Research. 2014; 42: D92–D97. https://doi.org/10.1093/nar/gkt1248.

[17] Zhou KR, Liu S, Sun WJ, Zheng LL, Zhou H, Yang JH, *et al*. ChIPBase v2.0: decoding transcriptional regulatory networks of non-coding RNAs and protein-coding genes from ChIP-seq data. Nucleic Acids Research. 2017; 45: D43–D50. https://doi.org/10.1093/nar/gkw965.

[18] Davis AP, Grondin CJ, Johnson RJ, Sciaky D, Wiegers J, Wiegers TC, *et al*. Comparative Toxicogenomics Database (CTD): update 2021. Nucleic Acids Research. 2021; 49: D1138–D1143. https://doi.org/10.1093/nar/gkaa891.

[19] Berman HM, Westbrook J, Feng Z, Gilliland G, Bhat TN, Weissig H, *et al*. The Protein Data Bank. Nucleic Acids Research. 2000; 28: 235–242. https://doi.org/10.1093/nar/28.1.235.

[20] Morris GM, Huey R, Lindstrom W, Sanner MF, Belew RK, Goodsell DS, *et al*. AutoDock4 and AutoDockTools4: Automated docking with selective receptor flexibility. Journal of Computational Chemistry. 2009; 30: 2785–2791. https://doi.org/10.1002/jcc.21256.

[21] Eberhardt J, Santos-Martins D, Tillack AF, Forli S. AutoDock Vina 1.2.0: New Docking Methods, Expanded Force Field, and Python Bindings. Journal of Chemical Information and Modeling. 2021; 61: 3891–3898. https://doi.org/10.1021/acs.jcim.1c00203.

[22] Adasme MF, Linnemann KL, Bolz SN, Kaiser F, Salentin S, Haupt VJ, *et al*. PLIP 2021: expanding the scope of the protein-ligand interaction profiler to DNA and RNA. Nucleic Acids Research. 2021; 49: W530–W534. https://doi.org/10.1093/nar/gkab294.

[23] Tchanque-Fossuo CN, Monson LA, Farberg AS, Donneys A, Zehtabzadeh AJ, Razdolsky ER, *et al*. Dose-response effect of human equivalent radiation in the murine mandible: part I. A histomorphometric assessment. Plastic and Reconstructive Surgery. 2011; 128: 114–121. https://doi.org/10.1097/PRS.0b013e31821741d4.

[24] Jiang YH, Li X, Niu W, Wang D, Wu B, Yang CH. β-Sitosterol regulated microRNAs in endothelial cells against an oxidized low-density lipoprotein. Food & Function. 2020; 11: 1881–1890. https://doi.org/10.1039/C9FO01976F.

[25] Hosseini A, Razavi BM, Banach M, Hosseinzadeh H. Quercetin and metabolic syndrome: A review. Phytotherapy research : PTR. 2021; 35: 5352–5364. https://doi.org/10.1002/ptr.7144.

[26] Kandere-Grzybowska K, Kempuraj D, Cao J, Cetrulo CL, Theoharides TC. Regulation of IL-1-induced selective IL-6 release from human mast cells and inhibition by quercetin. British Journal of Pharmacology. 2006; 148: 208–215. https://doi.org/10.1038/sj.bjp.0706695.

[27] Danciu C, Avram S, Pavel IZ, Ghiulai R, Dehelean CA, Ersilia A, *et al*. Main Isoflavones Found in Dietary Sources as Natural Anti-inflammatory Agents. Current Drug Targets. 2018; 19: 841–853. https://doi.org/10.2174/1389450118666171109150731.

[28] Jingya Z, Peng L. Glycitein Mitigates Doxorubicin-Induced Cardiotoxicity by Mitigating Apoptosis and Inflammatory Responses in Albino Rats. Journal of Biochemical and Molecular Toxicology. 2025; 39: e70489. https://doi.org/10.1002/jbt.70489.

[29] Chen Y, Fang ZM, Yi X, Wei X, Jiang DS. The interaction between ferroptosis and inflammatory signaling pathways. Cell Death & Disease. 2023; 14: 205. https://doi.org/10.1038/s41419-023-05716-0.

[30] Kastenhuber ER, Lowe SW. Putting p53 in Context. Cell. 2017; 170: 1062–1078. https://doi.org/10.1016/j.cell.2017.08.028.

[31] Zhang G, Sun N, Li X. Spleen tyrosine kinase inhibition mitigates radiation-induced lung injury through anti-inflammatory effects and downregulation of p38 MAPK and p53. Frontiers in Oncology. 2024; 14: 1406759. https://doi.org/10.3389/fonc.2024.1406759.

[32] Schinke H, Shi E, Lin Z, Quadt T, Kranz G, Zhou J, *et al*. A transcriptomic map of EGFR-induced epithelial-to-mesenchymal transition identifies prognostic and therapeutic targets for head and neck cancer. Molecular Cancer. 2022; 21: 178. https://doi.org/10.1186/s12943-022-01646-1.

[33] Nair S, Bonner JA, Bredel M. EGFR Mutations in Head and Neck Squamous Cell Carcinoma. International Journal of Molecular Sciences. 2022; 23: 3818. https://doi.org/10.3390/ijms23073818.

[34] Van den bossche V, Vignau J, Vigneron, E. *et al*. PPARα-mediated lipid metabolism reprogramming supports anti-EGFR therapy resistance in head and neck squamous cell carcinoma. Nature Communications. 2025; 16: 1237. https://doi.org/10.1038/s41467-025-56675-3.